FLY-OVER NOISE MEASUREMENTS OF A DISTRIBUTED PROPULSION FLIGHT DEMONSTRATOR

R. Wickersheim*, M. Keßler*, E. Krämer*

* University of Stuttgart, Institute of Aerodynamics and Gas Dynamics, Wankelstraße 3, Stuttgart, Germany

Abstract

In this study, fly-over noise measurements were conducted on a flight demonstrator equipped with distributed propulsion. Five distinct fly-over scenarios were executed, with noise data captured using an acoustic array. By utilizing GPS data and flight speed data, the noise signature of each fly-over was analyzed by segmenting the time signal into multiple sections. Furthermore, due to background noise, frequency ranges containing the blade passing frequencies were filtered from the raw signal. Combining the GPS, flight speed and acoustic data allowed for the reconstruction of noise carpets. The results show that all noise carpets exhibited a similar directivity pattern, with a distinct region of higher noise emission. Additionally, a background noise cancellation method was introduced, which did not affect the observed frequency range.

Keywords

Distributed Electric Propulsion; Acoustic Measurements; Aeroacoustics

NOMENCLATURE

Symbolds

c	Wing chord	m
D	Propeller diameter	m
J	Advance ratio	-
p	Sound pressure	Pa
R	Propeller radius	m
T	Propeller thrust	N
u, v, w	Velocity components	m/s
x, y, z	Aircraft coordinates	m

Abbreviati	ons	
Alt	Altitude	
BPF	Blade passing frequency	
DEP	Distributed Propulsion	
FO	Fly-over	
LAT	Latitude decimal degree	0
LONG	Longitude decimal degree	0
Mic	Microphone	
SPL	Sound Pressure Level	dB

1. INTRODUCTION

To achieve the goal of climate-neutral aircraft propulsion, innovative concepts are being developed, including distributed electric propulsion (DEP) [1]. Hereby, numerous smaller propellers are distributed over the wing span instead of one or two main propellers, with an advantage regarding lift increase due to the propeller slipstream [2, 3]. However, the interactions among the propellers and wing cause several noise mechanisms, which are not fully understood yet. In wind tunnel tests and numerical simulations it was shown that propeller noise due to generated steady and unsteady loading as well as propeller-wing interaction noise arise as dominant [4-7]. Furthermore, propeller-wing interaction noise consists of several sub-components, for instance propeller-vortex interactions, potential field interactions and scattering effects [6, 8].

Though these effects are investigated on generic setups, the investigation under real flight condition is unknown. Hence, the LuFo VI-1 research project VELAN deals with the investigation of the scaled flight demonstrator e-Genius-Mod equipped with DEP [9]. The aerodynamic and acoustic behavior of a flying DEP system is demonstrated in flight tests and will be compared to numerical simulations in the future. Thus, the scope of this paper is to determine the noise emissions of the flight demonstrator using a ground microphone array, comparable to measurements already applied in the literature [10, 11]. This will close the gap between the generic observations made in the literature to a real flying DEP-system.

2. SETUP

2.1. e-Genius-Mod

Within the LuFo VI-1 research project VELAN, the flight demonstrator e-Genius-Mod is equipped with distributed propellers along the wing span, see Fig. 1. The e-Genius-Mod has a wing span of $4.66\,\mathrm{m}$, a length of $2.7\,\mathrm{m}$ and a maximum take-off mass of $40\,\mathrm{kg}$. The inner section of the un-tapered wing exhibits a wing chord length of $c=0.3165\,\mathrm{m}$. For further details on the test platform, reference is made to the literature [9]. The 5-bladed Ramoser propellers with a diameter of 10 inches are mounted in tractor configuration with a distance to the leading edge of the wing in horizontal direction of $x_P/c = -40\%$ and a propeller spacing in spanwise direction of $y_P/D = 25\%$. While the wingtip mounted propeller has no vertical shift, the inner propellers are shifted $z_P/R = -30\%$ with an inclination angle of 8°, based on aerodynamic studies. To fulfil the take-off thrust requirement of 20 N per propeller the pitch is adjusted to 22.5° at r/R = 70%.



FIG 1. e-Genius-Mod in DEP configuration.

Overall, eight counter-rotating propellers are installed, with four per half span of the aircraft. Hereby, the propellers are numbered from one to four, accordingly from the wingtip to the inner section of the wing, as illustrated in Fig. 2.

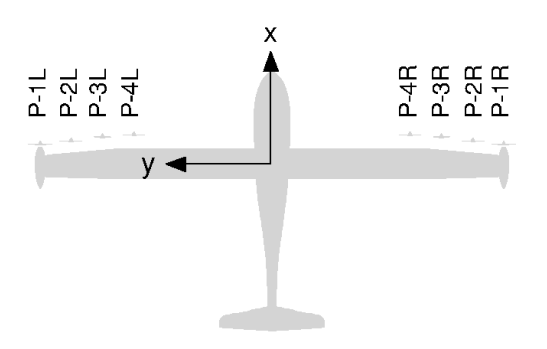


FIG 2. Propeller designation.

2.2. Ground Microphone Array

The ground microphone array comprises 14 beyerdynamic MM1 microphones with a distance of $2.5\,\mathrm{m}$ to each other placed upside down on a steel plate, as illustrated in Fig. 3. Overall, the microphone array

width amounts to $30\,\mathrm{m},$ to capture a sufficient range of noise directivity. The microphones are fixed by a tripod to ensure a distance of $5\,\mathrm{mm}$ between the microphone and the ground plate. Thus, a defined total reflection of the sound pressure waves can be assumed, leading to an amplitude amplification of +6 $\mathrm{dB}.$



FIG 3. Microphone placed on ground plate.

The microphone array is placed on the grass runway of the airport in Mengen, ensuring the mitigation of side reflections on the ground. Each microphone is connected with a measurement box, collecting the time signal of the sound pressure. Overall 5 acoustic boxes are used with four or two channels each, see Fig. 4. The acoustic boxes communicate via WLAN to the measurement PC, enabling a live tracking of noise emissions at fly-over.



FIG 4. Acoustic setup.

Just before the flight tests, each microphone is calibrated with a $1000\,\mathrm{Hz}$ signal emitting a defined sound wave with a $94\,\mathrm{dB}\text{-amplitude}.$ Thus, the measurement accuracy can be considered equivalent to that of the calibrator.

2.3. Time Synchronization

A DCF77-like signal is used to synchronize the absolute measurement time of each microphone and the measurements provided by e-Genius-Mod's logging [12]. Therefore, an in-house developed signal transmitter is used, emitting the signal of the DCF77 coding including the time information, received by each microphone, see Fig. 5. To guarantee a full signal information of the absolute time, it is ensured that the received time is of the length of at least one minute. Thus, the absolute time of each microphone is determined by decoding individually the binary code provided by the signal. In combination with the time logged from the aircraft, the relative position of

each microphone can be calculated, which will be discussed later in this paper.

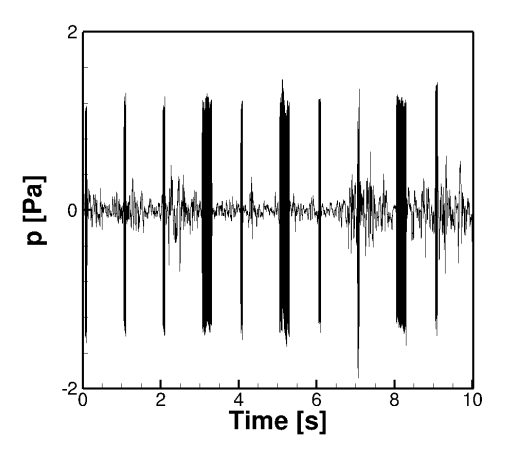


FIG 5. Time history of the DCF77 signal.

3. METHODOLOGY

In sum, five fly-over (FO) maneuvers are manually performed, while the trajectory of each fly-over is tracked by GPS sensors, providing additional information of the absolute time at each point, propeller data and aerodynamic data. The procedure to obtain and post-process these data is described in this section.

3.1. GPS Data

The GPS data of the aircraft is logged by the integrated Pixehawk 4 with a frequency of $10\,\mathrm{Hz}$ as well as from the additionally integrated acoustic measurement system in the e-Genius-Mod, which serves as backup.

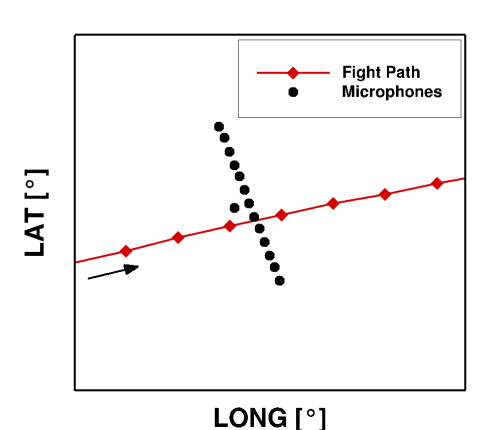


FIG 6. Flight path of fly-over #5.

Additionally, the GPS position of each microphone is tracked before the measurements. The placement of the microphone array relative to the flight path is shown in Fig. 6. Since the real position of the GPS data is somehow imprecise, the position is measured additionally per hand and further the GPS data are smoothed to meet the measured distance of $2.5\,\mathrm{m}$

and two individually measured positions of the array. Subsequently, the relative distance to the aircraft can be determined in flight (x) and spanwise (y) direction with Eq. 1 and 2.

(1)
$$\Delta x = 71.5 \cdot (LONG_{eGenius} - LONG_{Mic}) \cdot 1000$$

(2)
$$\Delta y = 111.3 \cdot (\text{LAT}_{\text{eGenius}} - \text{LAT}_{\text{Mic}}) \cdot 1000$$

By determining the intersection of both paths, the location and absolute time of the fly-over incident is defined.

3.2. Flight Conditions

Flight speed is measured by a straight 5-hole probe from Vectoflow mounted at the e-Genius-Mod. The raw signal includes unphysical outliers, thus the $2\,\mathrm{s}$ -signal is filtered. For this, the standard deviation is determined with the filter width being two times the standard deviation in each direction. The averaged values of the filtered signal are tabulated in Tab. 1 for each fly-over scenario. Furthermore, the altitude of the aircraft is provided by the Pixehawk 4, which is averaged for each fly-over. Since the flight path of FO 3 was not directly above the microphone array, this scenario is excluded from the investigation, since no usable acoustic signals are obtained.

TAB 1. Flight Condition.

	u [m/s]	v [m/s]	w [m/s]	alt. [m]
FO 1	39.96	1.44	2.88	5.19
FO 2	40.52	1.61	2.81	3.6
FO 3	-	-	-	-
FO 4	38.15	2.14	3.36	6.02
FO 5	37.59	2.04	3.378	3.36

3.3. Propeller Data

Lastly, propeller rotational speeds are measured and post-processed in the same manner as described in Sec. 3.2.

TAB 2. Propeller RPM - right wing span.

	P-1R [RPM]	P-2R [RPM]	P-3R [RPM]
FO 1	9596	9903	9452
FO 2	9483	9852	9431
FO 3	-	-	-
FO 4	9459	9736	9309
FO 5	9412	9676	9265

Due to the limited weight of the vehicle, solely three rotational speed measurement systems are integrated, see Tab. 2.

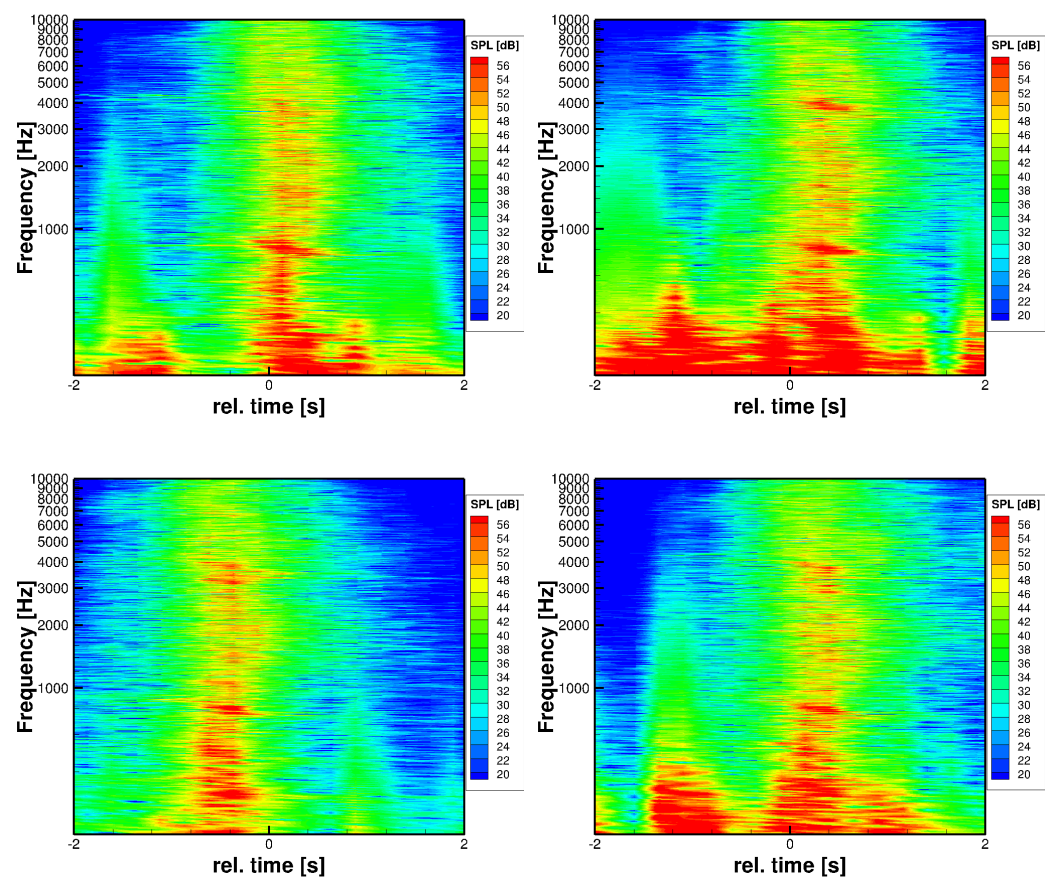


FIG 7. Spectral analysis of fly-over noise - FO 1 (upper left), FO 2 (upper right), FO 4 (lower left) and FO 5 (lower right).

The propellers are not controlled regarding their rotational speed but are provided with the same motor power. It can be seen that for all three propellers a comparable rotational speed was achieved, and it is assumed that the other rotational speeds are in an equivalent range.

4. ACOUSTIC EVALUATION

4.1. Spectral Analysis

At first, a spectral analysis of the distinct fly-overs is provided. Therefore, the acoustic signals of the ground microphones are processed as follows. Using the absolute time correlation of the e-Genius-Mod GPS signal and the time synchronization done before, the time of incidence is determined. Additionally, due to the speed of the aircraft, an observer time window for each fly-over is defined, prescribed to $\Delta t = 10 \, \mathrm{s}$. This time window is further divided into time sections of length $\Delta t = 0.25\,\mathrm{s}$ to discretize the time and to adequately capture fly-over noise with a sufficient frequency resolution. It was verified that this time discretization is the optimal choice, comparing it to time steps of different lengths. Hereby, due to the short length of the time section, the frequency resolution results in $\Delta f = 4 \, \mathrm{Hz}$. For each time section, an FFT analysis is performed, to identify the spectral components. For visualization purposes, the time section of 2s is shown in Fig. 7 as spectrogram for the center microphone, with $t = 0 \, \mathrm{s}$ being the time, when the aircraft passes the microphone array. It can be seen that for all fly-overs the noise, especially above a frequency of $200\,\mathrm{Hz}$, increases. Due to the rotational speed of the propellers and the blade count, a range of frequencies, including the blade passing frequencies, occur around $800\,\mathrm{Hz}$. For each fly-over this distinct region as well as higher harmonics can be seen. In the low frequency region, the noise is dominated by background noise for fly-over 1,2 and 5. Nevertheless, since the region of the BPFs is of major interest for this work, the lower frequencies can be omitted, while at the frequencies including the BPF no significant background noise was observed. Since the aircraft has not the exact same position in each fly-over, the distance to the center microphone varies, explaining the time shift of the spectrogram.

4.2. Frequency-Filtered Flyover Noise

In the next step, the shown acoustic signals are filtered according to their BPFs. Since the aircraft is moving relative to the fixed microphone array, the Doppler shift effect is not negligible. Therefore, the minimum and maximum frequencies for each

scenario are determined as described in Eq. 3 and 4. For this purpose, the minimum frequency is based on the lowest RPM existing in the respective fly-over, while vice versa for the maximum frequency. Furthermore, the Doppler shift is determined using the airspeed information shown previously. Here, solely the x-component of the velocity is considered. To define the minimum frequency, the Doppler shift is subtracted from the resulting frequency, while for the maximum frequency it is added.

(3)
$$f_{\min} = \frac{\min|\text{RPM}|}{60} \cdot n_{\text{Blades}} \cdot (1 - \frac{u}{c})$$

(4)
$$f_{\text{max}} = \frac{\text{max}|\text{RPM}|}{60} \cdot n_{\text{Blades}} \cdot (1 + \frac{u}{c})$$

Thus, the following frequency ranges result for the filtering. To calculate the SPL from the filtered signal, all spectral contributions are added up. The resulting SPLs are only considering the first BPF and exclude all other frequencies, which might include background noise or spurious noise.

TAB 3. Frequency Ranges.

	f_{\min} [Hz]	$f_{ m max}$ [Hz]
FO 1	695	922
FO 2	692	918
FO 3	-	-
FO 4	689	902
FO 5	687	895

The frequency-filtered SPL for the center microphone over the fly-over time is illustrated in Fig. 8.

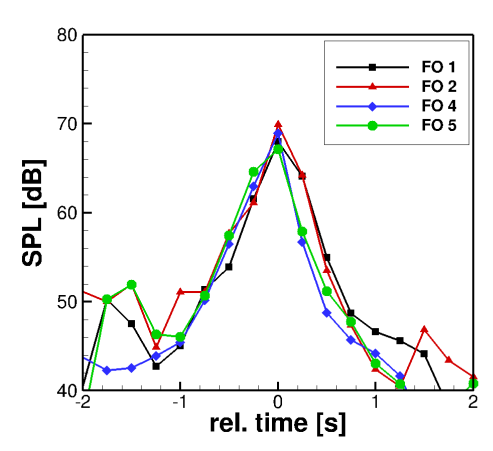


FIG 8. Fly-over noise of center microphone.

It can be seen that with decreasing distance to the microphone the SPL increases as expected. The characteristic of the fly-over noise is similar for all scenarios, while they differ obviously in magnitude due to the different distances. As already expected from the spectrogram, FO 4 exhibits the lowest background

noise, resulting in lower noise before and after the flyover time.

4.3. Background Noise Cancellation

It was shown previously that background noise is not a major concern in the relevant frequency range. Nevertheless, a method for background noise cancellation is introduced. Therefore, a time window of $\Delta t=1\,\mathrm{s}$ is chosen for background noise determination. It is assumed from the previous results that the usable signal for the center microphone is $1\,\mathrm{s}$ before the fly-over. The defined background noise is processed similar to the usable signal.

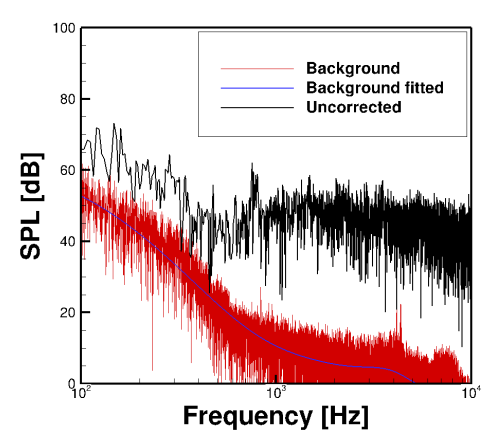


FIG 9. Background noise. at $t=-1\,\mathrm{s}$

The resulting spectrum of the background noise is further smoothed using a spline function, cancelling stochastic components of the signal. The FFT analysis of the usable noise and background noise is illustrated in Fig. 9 for FO 1 as example. If the difference exceeds $10\,\mathrm{dB}$, background noise is subtracted from the usable signal. As mentioned, it can be seen that background noise is significantly lower in the frequency range around $800\,\mathrm{Hz}$, thus background noise cancellation is not needed. Nevertheless, for lower frequencies this method can improve the quality of the noise signal.

4.4. Reconstruction of Noise Carpet

Finally, noise carpets from the obtained acoustic fly-over signals are reconstructed. Therefore, the relative time is multiplied with the flight speed to receive the relative x-position to the microphones. Additionally, the spanwise positions are determined from the GPS data for each microphone. sequently, the frequency-filtered noise levels are interpolated and mapped on a carpet extending 20 m in every direction. This enables the direct comparison of the fly-over scenarios, since a quantitative comparison of each microphone is not possible, due to the different distances. The discretization in flight direction is limited through the flight speed. resulting in $\Delta x = 10 \,\mathrm{m}$, while the spanwise direction shows a finer resolution of $\Delta y = 2.5\,\mathrm{m}$. The origin

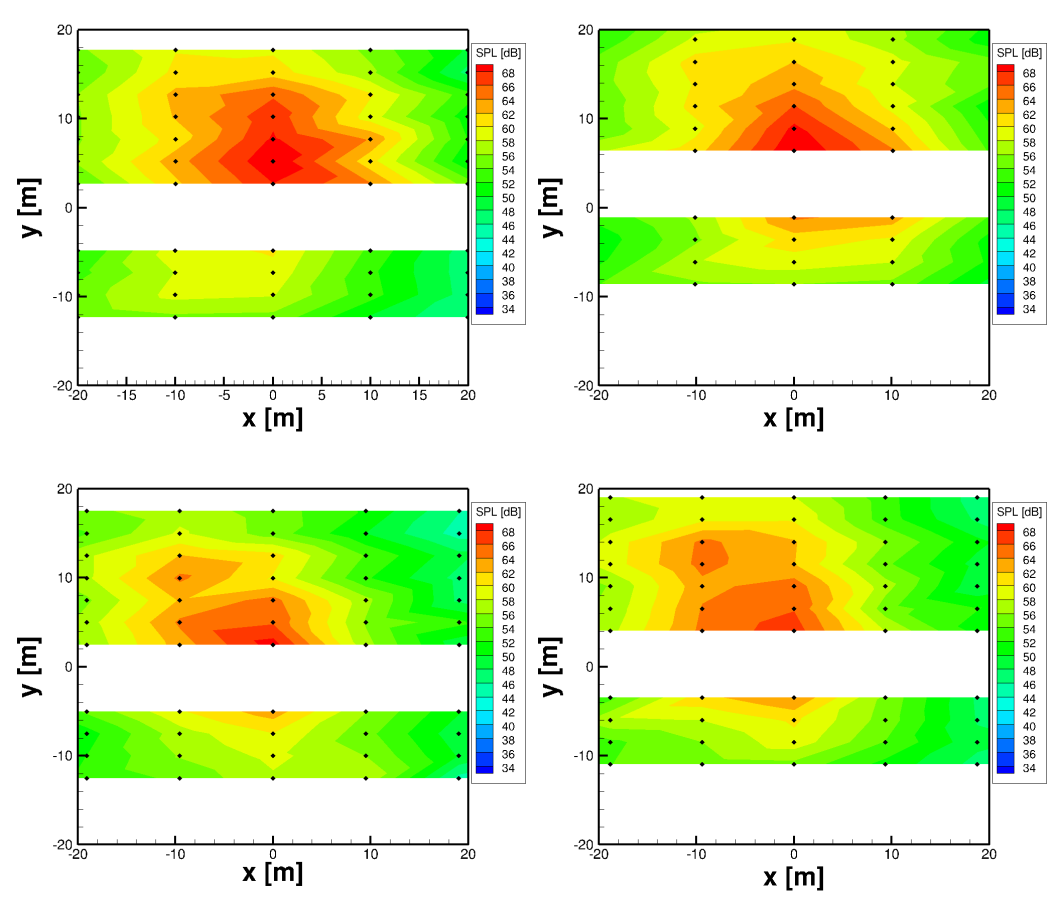


FIG 10. Noise carpet of fly-over data - FO 1 (upper left), FO 2 (upper right), FO 4 (lower left) and FO 5 (lower right).

of the noise carpet corresponds to the origin of the aircraft. Thus, the extension of the noise carpet in negative spanwise direction is lower than in positive direction due to the flight trajectory. Due to a failure, two microphones were unable to record during the flight tests. Therefore, the corresponding regions in the reconstructed noise carpet are blanked. All fly-overs show a clear maximum in SPL below the aircraft, with similar noise directivity. It is assumed that the slight asymmetry of the maximum noise is due to the uncertainty of the GPS position of the aircraft. Additionally, the magnitude of the noise is in a similar range, nevertheless, differs due to the different heights of the fly-overs. By considering this qualitative view, it becomes evident that the fly-over characteristics are sufficiently reproducible with solely minor differences. Also the sensitivity of marginal differences in flight condition, i.e. flight speed and rotational speed, can be seen on the noise emission.

5. CONCLUSION & OUTLOOK

Within this work, fly-over noise measurements with a ground microphone array were carried out to capture noise directivity of a distributed propulsion system. Therefore, the existing test platform e-Genius-Mod was equipped with eight electrically driven propellers. Beside the noise measurements, GPS and airspeed was tracked to support the acoustic measurements

and determine the relative distance to the array. By using the frequency range containing the first BPFs of the propellers, a clear fly-over noise characteristic was observed. These noise signature were reconstructed to a noise carpet to capture the noise directivity of each fly-over. It was found that all fly-overs show a similar noise directivity.

This study serves as comparison basis for numerical simulations and presents a method for evaluating the noise signals of a DEP-system. Furthermore, it demonstrates a method of extracting tonal noise from background noise, since the noise signature of a scaled flight demonstrator is significantly lower than for full-scale. Future research will focus on the numerical simulation of the presented fly-over scenarios to compare the tonal noise directivity, extending the understanding of DEP noise under real flight conditions.

Contact address:

robin.wickersheim@iag.uni-stuttgart.de

Acknowledgment The authors gratefully acknowledge the Federal Ministry for Economic Affairs and Climate Action (BMWK) for funding this work in the framework of the research project VELAN (FKZ: 20E1919).



References

- [1] Hyun D. Kim, Aaron T. Perry, and Phillip J. Ansell. A Review of Distributed Electric Propulsion Concepts for Air Vehicle Technology. AIAA/IEEE Electric Technologies Symposium, 2018. DOI: https://doi.org/10.2514/6.2018-4998.
- [2] Karen A. Deere, Sally A. Viken, Melissa B. Carter, and Jeffrey K. Viken. Computational Analysis of Powered Lift Augmentation for the LEAPTech Distributed Electric Propulsion Wing. AIAA Aviation Denver, 2017. DOI: https://doi.org/10.2514/6.2017-3921.
- [3] Mário Firnhaber Beckers, Michael Schollenberger, Thorsten Lutz, Dustin Bongen, Rolf Radespiel, Juan L. Florenciano, and David E. Funes-Sebastian. Numerical Investigation of High-Lift Propeller Positions for a Distributed Propulsion System. *Journal of Aircraft*, June 2023. DOI: https://doi.org/10.2514/1.C037248.
- [4] Robin Wickersheim, Manuel Keßler, and Ewald Krämer. Noise Prediction of a Distributed Propulsion System Using the Actuator Line Method. AIAA Journal, March 2024. DOI: https://doi.org/10.2514/1.J063457.
- [5] Robin Wickersheim, Manuel Keßler, and Ewald Krämer. Aeroacoustics of High Fidelity URANS Simulations of Distributed Electric Propellers. New Results in Numerical and Experimental Fluid Mechanics XIV, July 2023. DOI: https://doi.org/10.1007/978-3-031-40482-5 33.
- [6] Robin Wickersheim, Manuel Keßler, Julia Sembowski, Dustin Bongen, and Jorge P. Gomes. Numerical Investigation and Validation of Noise Sources of a Distributed Propulsion System. AIAA/CEAS Aeroacoustics Conference, June 2024. DOI: https://doi.org/10.2514/6.2024-3208.
- [7] Deepak C. Akiwate, Anthony Parry, Phillip Joseph, and Chaitanya C. Paruchuri. Analytical Investigation of Propeller-Wing Interaction Noise. AIAA/CEAS Aeroacoustics Conference, Southampton, UK, 2022. DOI: https://doi.org/10.2514/6.2022-2877.
- [8] Jack E. Barker, Alessandro Zarri, Julien Christophe, and Christophe F. Schram. Numerical Investigation of Tonal Noise Emissions

- from Propeller-Wing Aerodynamic and Acoustic Interactions. *AIAA Aviation Forum*, June 2023. DOI: https://doi.org/10.2514/6.2023-4056.
- [9] Dominique P. Bergmann, Jan Denzel, Asmus Baden, Lucas Kugler, and Andreas Strohmayer. Innovative Scaled Test Platform e-Genius-Mod Scaling Methods and Systems Design. Aerospace, 2019. DOI: https://doi.org/10.3390/aerospace6020020.
- [10] Ulrich Kowarsch, Constantin Oehrle, Manuel Keßler, and Ewald Krämer. Aeroacoustic Simulation of a Complete H145 Helicopter In Descent Flight. *Journal of the American Helicopter Society*, 2016. DOI: https://doi.org/10.4050/JAHS.61.042001.
- [11] Gert Herold and Ennes Sarradj. Characterizing Multicopter UAV Noise Emission Through Outdoor Fly-by Measurements with a Microphone Array. AIAA/CEAS Aeroacoustics Conference, June 2024. DOI: https://doi.org/10.2514/6.2024-3332.
- [12] Dirk Piester, Peter Hetzel, and Andreas Bauch. Zeit- und Normalfrequenzverbreitung mit DCF77. *PTB-Mitteilungen 114*, 2004.